

A Measurement of the  $D^{*\pm}$  Cross Section in Two-Photon Processes \*

TOPAZ Collaboration

R.Enomoto<sup>(1)†</sup>, M.Iwasaki<sup>(2)</sup>, K.Muramatsu<sup>(2)</sup>, H.Hayashii<sup>(2)</sup>, A.Miyamoto<sup>(1)</sup>, R.Itoh<sup>(1)</sup>, K.Abe<sup>(3)</sup>,  
 T.Abe<sup>(4)</sup>, I.Adachi<sup>(1)</sup>, M.Aoki<sup>(4)</sup>, S.Awa<sup>(2)</sup>, R.Belusevic<sup>(1)</sup>, K.Emi<sup>(3)</sup>, H.Fujii<sup>(1)</sup>, K.Fujii<sup>(1)</sup>, T.Fujii<sup>(5)</sup>,  
 J.Fujimoto<sup>(1)</sup>, K.Fujita<sup>(6)</sup>, N.Fujiwara<sup>(2)</sup>, B.Howell<sup>(7)</sup>, N.Iida<sup>(1)</sup>, H.Ikeda<sup>(1)</sup>, H.Iwasaki<sup>(1)</sup>,  
 R.Kajikawa<sup>(4)</sup>, S.Kato<sup>(8)</sup>, S.Kawabata<sup>(1)</sup>, H.Kichimi<sup>(1)</sup>, M.Kobayashi<sup>(1)</sup>, D.Koltick<sup>(7)</sup>, I.Levine<sup>(7)</sup>,  
 K.Miyabayashi<sup>(4)</sup>, K.Nagai<sup>(9)</sup>, T.Nagira<sup>(2)</sup>, E.Nakano<sup>(4)</sup>, K.Nakabayashi<sup>(4)</sup>, O.Nitoh<sup>(3)</sup>, S.Noguchi<sup>(2)</sup>,  
 F.Ochiai<sup>(10)</sup>, Y.Ohnishi<sup>(4)</sup>, H.Okuno<sup>(8)</sup>, T.Okusawa<sup>(6)</sup>, K.Shimozawa<sup>(4)</sup>, T.Shinohara<sup>(3)</sup>, A.Sugiyama<sup>(4)</sup>,  
 N.Sugiyama<sup>(11)</sup>, S.Suzuki<sup>(4)</sup>, K.Takahashi<sup>(3)</sup>, T.Takahashi<sup>(6)</sup>, M.Takemoto<sup>(2)</sup>, T.Tanimori<sup>(11)</sup>,  
 T.Tauchi<sup>(1)</sup>, F.Teramae<sup>(4)</sup>, Y.Teramoto<sup>(6)</sup>, N.Toomi<sup>(2)</sup>, T.Toyama<sup>(4)</sup>, T.Tsukamoto<sup>(1)</sup>, S.Uno<sup>(1)</sup>,  
 Y.Watanabe<sup>(11)</sup>, A.Yamaguchi<sup>(2)</sup>, A.Yamamoto<sup>(1)</sup>, and M.Yamauchi<sup>(1)</sup>

<sup>(1)</sup> *National Laboratory for High Energy Physics, KEK, Ibaraki-ken 305, Japan*

<sup>(2)</sup> *Department of Physics, Nara Women's University, Nara 630, Japan*

<sup>(3)</sup> *Dept. of Applied Physics, Tokyo Univ. of Agriculture and Technology, Tokyo 184, Japan*

<sup>(4)</sup> *Department of Physics, Nagoya University, Nagoya 464, Japan*

<sup>(5)</sup> *Department of Physics, University of Tokyo, Tokyo 113, Japan*

<sup>(6)</sup> *Department of Physics, Osaka City University, Osaka 558, Japan*

<sup>(7)</sup> *Department of Physics, Purdue University, West Lafayette, IN 47907, USA*

<sup>(8)</sup> *Institute for Nuclear Study, University of Tokyo, Tokyo 188, Japan*

<sup>(9)</sup> *The Graduate School of Science and Technology, Kobe University, Kobe 657, Japan*

<sup>(10)</sup> *Faculty of Liberal Arts, Tezukayama Gakuin University, Nara 631, Japan*

<sup>(11)</sup> *Department of Physics, Tokyo Institute of Technology, Tokyo 152, Japan*

**Abstract**

We have measured the inclusive  $D^{*\pm}$  production cross section in a two-photon collision at the TRISTAN  $e^+e^-$  collider. The mean  $\sqrt{s}$  of the collider was 57.16 GeV and the integrated luminosity was  $150 \text{ pb}^{-1}$ . The differential cross section ( $d\sigma(D^{*\pm})/dP_T$ ) was obtained in the  $P_T$  range between 1.6 and 6.6 GeV and compared with theoretical predictions, such as those involving direct and resolved photon processes.

Hadron production in two-photon collisions is described by the vector-meson dominance model, the quark-parton model (direct process) [1], and the hard scattering of the hadronic constituents of almost-real photons (resolved photon process) [2, 3, 4, 5], which has been observed by the previous experiments [6]. However, more detailed studies are necessary in order to understand these processes quantitatively. Heavy quark pair production processes are good probes, since the theoretical calculations are less ambiguous than for light quarks[7].

The previous measurements had been carried out at around  $\sqrt{s} \sim 30 \text{ GeV}$  [8, 9, 10], and are consistent with a recent theoretical prediction[7]. At the TRISTAN energy ( $\sqrt{s} \sim 60 \text{ GeV}$ ), the  $c\bar{c}$  production cross section becomes sizable; we have obtained the largest statistics for this type of process. We carried out a measurement of the  $D^{*\pm}$  production cross section at a  $P_T$  greater than 1.6 GeV in two-photon collision events.

The detail concerning the TOPAZ detector can be found elsewhere [11]. The integrated luminosity of the event sample used in the analysis was  $150 \text{ pb}^{-1}$ . The mean  $\langle \sqrt{s} \rangle$  of the collider was 57.16 GeV. The trigger conditions are as follows: more than two tracks with  $P_T > 0.3 \sim 0.7 \text{ GeV}$  and opening angle

\* published in Phys. Rev. **D 50**, 1879 (1994).

†internet address: enomoto@kekvax.kek.jp

> 45~70 degrees (depending on the beam condition); a neutral energy deposit in the barrel calorimeter be greater than 4 GeV; or that in the endcap calorimeters be greater than 10 GeV.

The selection criteria for two-photon events are as follows: the number of charged tracks be  $\geq 4$ ; the total visible energy in the central part of the detector be between 4 and 25 GeV; the vector sum of the transverse momenta of the particles with respect to the beam axis ( $|\Sigma \vec{P}_T|$ ) be less than 7.5 GeV; the sum of the charges be  $\leq 3$ ; the event vertex be consistent with the beam crossing point; and no large energy clusters ( $E > 0.25E_{beam}$ ) in the barrel calorimeter. In addition, we divided each event into two jets with respect to the plane perpendicular to the thrust axis, and the cosine of the angle between the two jets was required to be greater than -0.9. These restrictions were made in order to reduce beam-gas, and single-photon-exchange events. A total of 10788 events was selected.

The charged track selections were as follows: the closest approach to the event vertex be consistent within the measurement error; the number of degrees of freedom (DOF) in the track-fitting be  $\geq 3$ ; and  $P_T$  be  $\geq 0.15$  GeV.

The  $\gamma$  selections were: the cluster be detected by a barrel-type lead-glass calorimeter; the energy be  $\geq 0.2$  GeV; and the cluster position be separated from any charged-track extrapolations. In addition, the  $e^+e^-$  pairs which were consistent with  $\gamma$  conversion at the inner vessel of the Time Projection Chamber (TPC) were reconstructed (1C-fit) and used as  $\gamma$  candidates.

In order to reconstruct charm quarks, we used the decay modes  $D^{*\pm} \rightarrow \pi^\pm D^0(\bar{D}^0)$ , followed by ( $D^0(\bar{D}^0) \rightarrow K^\mp \pi^\pm X(\bar{X})$ ). From now on, any mention of decays includes the charge conjugation modes, for simplicity. For  $D^0$  decays, the decay modes  $D^0 \rightarrow K^-\pi^+$ ,  $K^-\pi^+\rho^0$ ,  $K^-\pi^+\pi^0$  ( $K^{*-}\pi^+$ ,  $K^-\rho^0$ ,  $\bar{K}^{*0}\pi^0$ ), and  $K^-\pi^+\pi^0\pi^0$  were reconstructed by using kinematical constraint fits (1-3C). The cuts on  $\chi^2_{fit}$  were required to be greater than the 5% confidence level (CL). These decay modes were selected because they have relatively high acceptances, considering the branching fractions and detector acceptances. For more than two-body decay modes, we applied a  $dE/dx$  cut in selecting  $K^-$ ; for a two-body decay, a sufficient S/N was obtained without this cut. The cuts on the vector meson masses were carried out according to the detector resolution and their intrinsic decay widths. In the case of vector-plus-pseudo-scalar decay, we applied cut on the angle of the decay product of the vector meson ( $\theta_{VP}$ ) in its center-of-mass frame with respect to the vector meson line of flight, i.e.,  $|\cos\theta_{VP}| > 0.5$ .

The  $D^{*+}$ s were reconstructed with those  $D^0$  candidates mentioned above while combining  $\pi^+$ s (soft-pions from hereafter) with momenta less than 0.65 GeV. The energy fraction,  $z = E(D^{*+})/E_{beam}$ , was required to be between 0.1 and 0.25. We then calculated the mass differences, i.e.,  $dM = M(\pi^+D^0) - M(D^0)$ . The  $dM$  distribution is plotted in Fig.1(a).

There were multi- $D^0$ -candidates for one soft-pion which gave similar  $dMs$ . These occurred when one of the lowest momentum particles of the  $D^0$  decay was misidentified[12]. In these cases, each entry gave similar  $dM$  value. The differences of  $dM$  values for pairs sharing the same soft-pions in the same events were plotted in Fig. 2. The peak around zero caused an overestimate of the statistical significance of the signal. In order to cure them, we carried out a weighting method, i.e., when there was more than one  $D^0$ -candidate for a given soft-pion, each entry in the  $dM$  histogram was weighted by the reciprocal of the number of candidates. By this procedure, we could avoid any overestimation of the statistical significance of the peak entry. This was checked using a Monte-Carlo simulation. The resulting  $dM$  distribution is shown in Fig. 1-(b). The mean visible energy at the rest frame (WVIS) for the events containing the  $D^{*\pm}$  candidates were 5.3 GeV. In order to check the peak around the  $D^{*\pm}$  region, we carried out the wrong-sign combination such as  $D^0\pi^-$  and etc. The results are plotted in Fig. 1-(c), (d), and (e). There were no peak structures at all. The excess below the  $D^{*\pm}$  peak was explained by the energy loss at support structures of the inner field cage and the central membrane of the TPC, which were distributed inhomogeneously, whereas the correction for them were made only in average. Figs 3 show the mass-differences of two cases: (a) when the soft-pion passed near these supports, and (b) when it passed far away from them. This happened because the soft-pions in the two photon events had extremely low momenta. We counted the entries of the higher  $dM$  peak as the  $D^{*\pm}$  yield in the experiment, and in

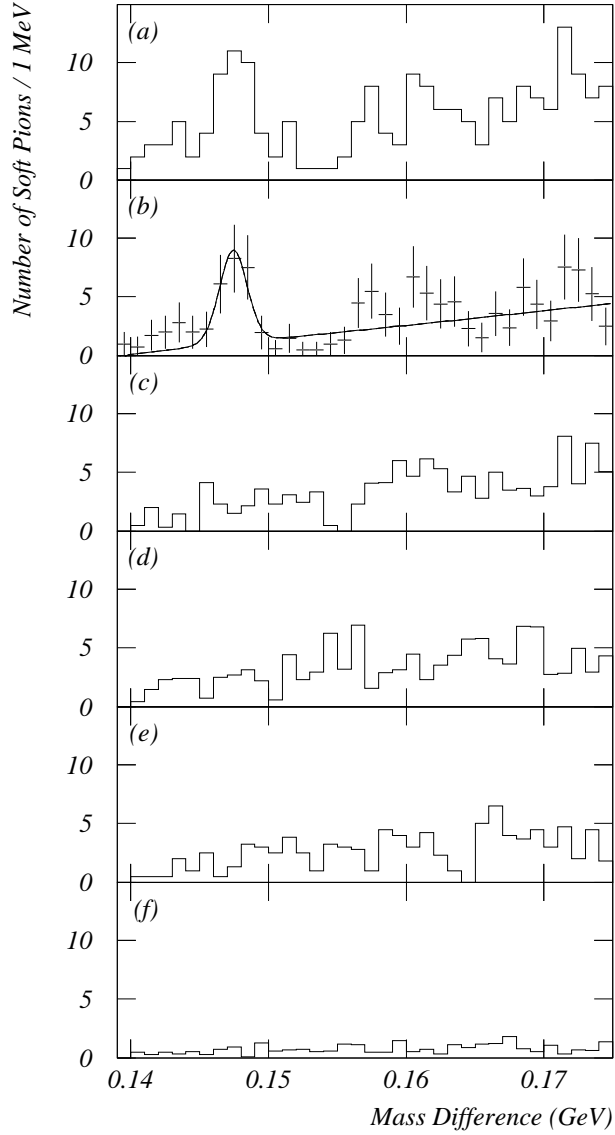


Figure 1: Mass-difference ( $dM = M(D^0\pi^\pm) - M(D^0)$ ) distributions: (a)  $dM$  distribution without the weighting; (b) after the weighting. The curve is obtained from a best-fit function described in the text; (c)  $dM$  distribution for wrong-sign soft-pion; (d) that for wrong-sign kaon; (e) that for wrong-sign soft-pion and wrong-sign kaon; and (f) background estimation from  $e^+e^- \rightarrow \gamma \rightarrow q\bar{q}$  processes.

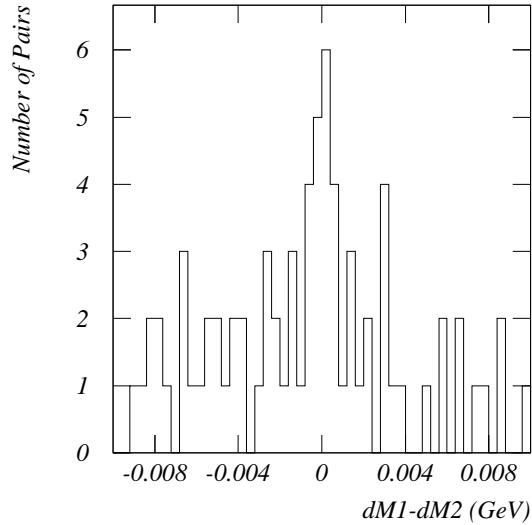


Figure 2: Differences of dM values for pairs sharing the same soft-pions in the same events.

the Monte-Carlo we corrected the peak entries about -15% considering the amount of the materials and their solid angle from the interaction point. The error of this correction was considered to be 5% which was estimated from the  $e^+e^-$  conversion pair yield in the two photon sample. Concerning the higher  $dM$  fluctuation, we have no explanations other than statistical fluctuations. The fitting function was the sum of a Gaussian and the following function:

$$a(dM - M(\pi^\pm))^b(1 - dM/c)^n,$$

where a, b, and c are free parameters and n is an average multiplicity of the event sample. The obtained  $D^{*\pm}$  yield was  $20.0 \pm 5.0$ , where the  $\chi^2$  of the fit was 31 with DOF=35. The peak position and its width obtained by this fitting were  $147.4 \pm 0.2$ , and  $0.8 \pm 0.2$  MeV, where the detector simulation predicted 145.4 and 1.6 MeV, respectively. We considered that the shift of the peak position was caused by the inhomogeneous material distribution described above, whereas the energy loss correction was carried out assuming uniform material. The shift of the mass-difference peak quantitatively agreed with the expectation. The resolution difference was due to the overestimation of the material in front of the TPC in the simulation in the most probable energy-loss case. 85% of the soft-pions were considered to pass away from the support structures of the TPC. We tried  $\chi^2$  and likelihood fitting and also tried polynomial background functions. The differences in the total  $D^{*\pm}$  yields were within 10%. Thus we concluded that the systematic error of the fitting procedure was 10%. The yields for the four decay modes described before were  $9.5 \pm 3.3$ ,  $4.8 \pm 2.3$ ,  $4.8 \pm 2.2$ , and  $0.9 \pm 0.9$ , respectively.

The background from  $e^+e^- \rightarrow \gamma \rightarrow q\bar{q}(\gamma)$  distributed smoothly in this  $dM$  plot (height was about 1 count a bin as shown in Fig. 1-(f)). No peak structures were obtained by the Monte-Carlo simulation. We also checked the event vertex distribution in order to determine the contamination of the beam-gas background. There was a clear peak at the interaction point with no tails.

In order to compare the experimental data with the theoretical prediction, we chose  $d\sigma(D^{*\pm})/dP_T$ , instead of the total cross section, as had been reported [8, 9, 10], since the accepted  $D^{*\pm}$  events were limited to the high  $P_T$  region due to the detector acceptance. We were sensitive to those  $D^{*\pm}s$  with transverse momenta ( $P_T$ ) between 1.6 and 6.6 GeV. The lower limit was due to the detector acceptance and the higher due to statistics. An acceptance correction was carried out by using a lowest-order (Born approximation) direct-process Monte-Carlo simulation, in which an equivalent photon approximation was

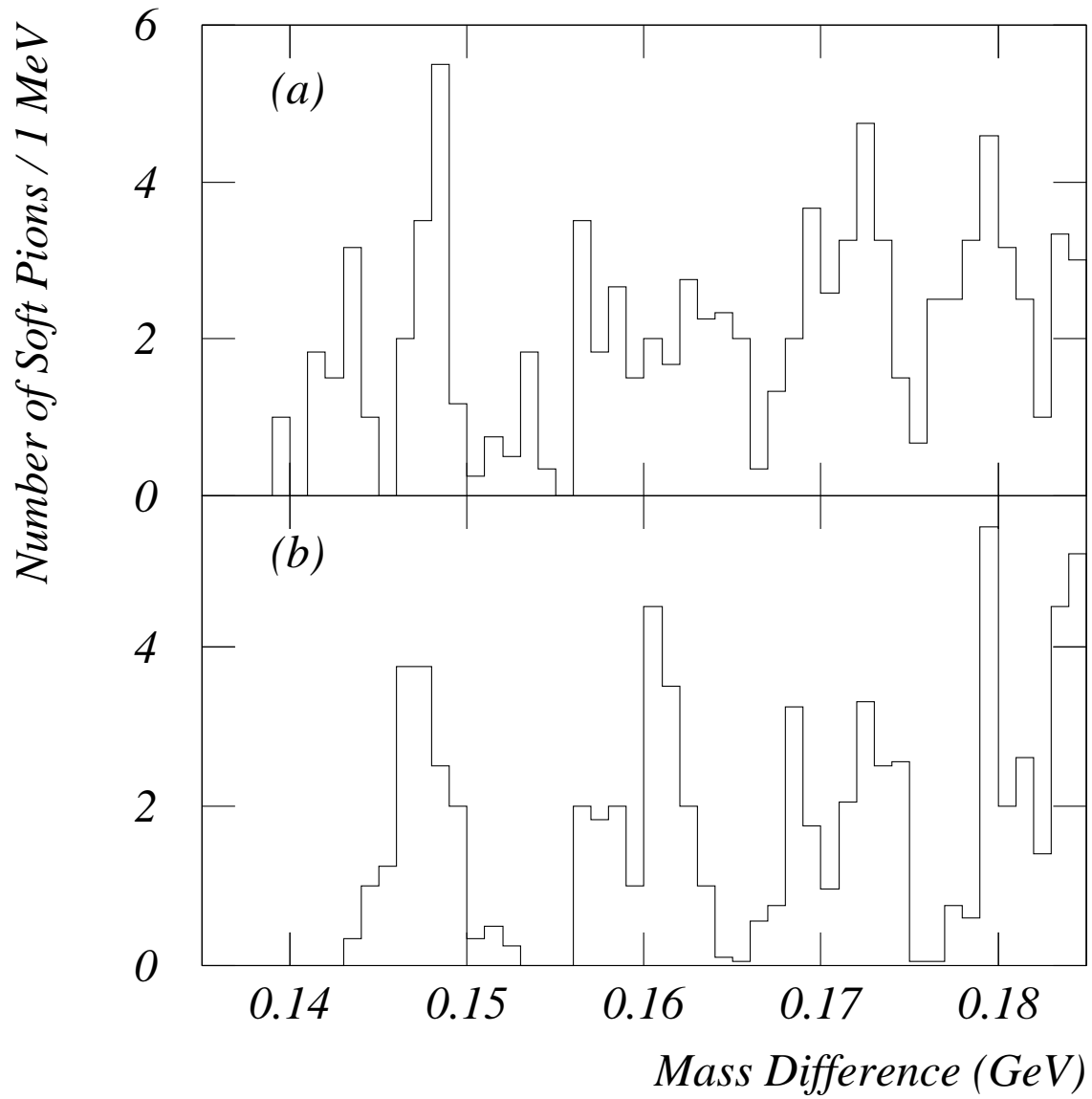


Figure 3: Mass-differences of two cases: (a) when the soft-pion passed near the TPC support structures, and (b) when it passed far away from them.

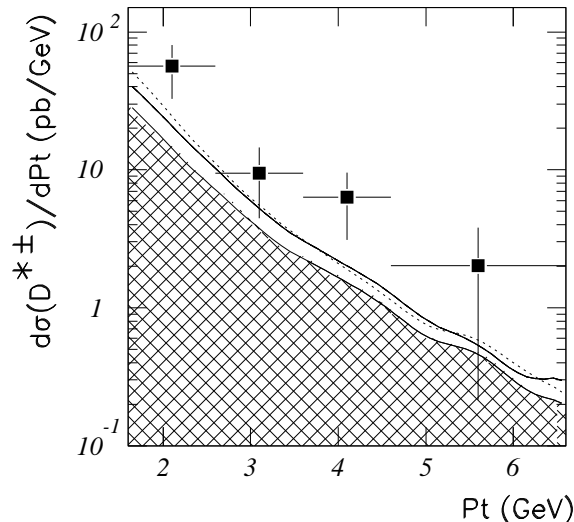


Figure 4:  $d\sigma(e^+e^- \rightarrow e^+e^- D^{*\pm} X)/dP_T$  versus  $P_T$ . The data points with error bars are the experimental data and the curves were obtained by Monte-Carlo simulations while assuming various processes. The hatched area is a prediction based on the direct process, the solid curve is based on a combination of direct and resolved photon process by the GRV parametrization, the dotted one is based on the LAC1 parameterization. The vertical scales for the resolved photon process were normalized by the relative acceptance to the direct process, because of the acceptance difference described in the text.

used. The  $P_T(D^{*\pm})$  smearing by the  $P_T$  of the initial photons was checked by a full calculation of the  $e^+e^- \rightarrow e^+e^-\gamma\gamma \rightarrow e^+e^-c\bar{c}$  process, and was concluded to be small. The hadronization was taken care of by LUND6.3 Monte-Carlo [13, 14]. We did not use a parton shower option in the LUND Monte-Carlo, since the choice of  $Q^2$  of the event was not well defined. The fragmentation parameters in the calculation have been tuned to reproduce the general properties of single-photon exchange processes. The systematic ambiguity for  $D^{*\pm}$  inclusive spectrum was considered to be at most 10 %. Because the fragmentation of the  $D^{*\pm}$  was measured well at various  $\sqrt{s}$  and the symmetric LUND fragmentation function reproduces it very well. The systematic uncertainty of the cross section is mostly due to the fitting procedure, fragmentation scheme (described so far), the branching ratios of  $D^0$  [15] and  $D^{*+}$  [16], the ambiguities in the detector acceptance and the calibrations. It was estimated to be 15%. The resulting differential cross sections are  $57 \pm 24$ ,  $9.5 \pm 5.1$ ,  $6.3 \pm 3.2$  and  $2.0 \pm 1.8$  pb/GeV (systematic errors included) for  $P_T$  regions 1.6-2.6, 2.6-3.6, 3.6-4.6, and 4.6-6.6 GeV, respectively, and are plotted in Fig. 4, together with the theoretical predictions. The raw entries at each  $P_T$  binnings were  $7.2 \pm 2.9$ ,  $6.4 \pm 3.3$ ,  $4.0 \pm 2.0$ , and  $2.4 \pm 2.1$ , where the errors are statistical error only, respectively.

Theoretical predictions for both direct and resolved photon processes were compared with this measurement as follows. In order to estimate  $\sigma(D^{*\pm})$  from the theoretical calculation of  $\sigma_{c\bar{c}}$ , we assumed  $P_{c \rightarrow D^{*\pm}} \times B(D^{*+} \rightarrow \pi^+ D^0) = 0.185 \pm 0.024$  at  $\sqrt{s} = 90$  GeV in Ref. [17]. This value is consistent with that obtained at  $\sqrt{s} = 10$  GeV [18]. The events were generated by the lowest-order calculations. The relative acceptance for the process of the resolved photon to that of the direct process was obtained to be  $0.76 \pm 0.25$  due to the event selection, where the error was especially due to the gluon-density function dependence. Although, this ambiguity is small compared with the total contribution including the direct process. Since we did not measure the energy flow in the low-angle region, spectator jets were not detected. This lower acceptance was especially due to the lower visible energy cut of 4 GeV. The vertical scale for the cross sections of the resolved photon process shown in Fig. 4 was normalized by this

factor.

Corrections of order  $\alpha_s$  were carried out according to the procedure in Ref. [19]. Since string fragmentation includes a parton-shower-like effect, the next-to-leading-order correction in the  $P_T$  spectrum is doubly counted. We used instead the  $P_T$ -independent correction to the direct process. The cross section of the direct process is increased by a factor of 1.31 uniformly, and that of the resolved photon process is corrected by a  $P_T$  dependent function, due to the presence of the process  $\gamma q \rightarrow c\bar{c}q$  (a part of this is absorbed in the gluon density function in the resolved photon). The  $P_T$  dependent factors were obtained by the following way: At first we derived the  $P_T$  dependent ratios between the higher and the lowest order calculations for the direct and resolved photon processes; we then calculated the factors between those of the direct and resolved photon process; and those factors were normalized to fit to the total cross section of the higher order calculations for the resolved photon process. The resulted  $P_T$  dependent correction were written as

$$0.50P_T^c + 0.54,$$

where  $P_T^c$  is a  $P_T$  of charm quark. The charm quark mass ( $m_c$ ) and the renormalization scale ( $\mu$ ) were assumed to be  $m_c=1.6$  GeV and  $\mu = \sqrt{2}m_c$ , respectively. The curves in Fig. 4 represent these predictions. The parametrization dependence for the resolved photon process appears in the lowest  $P_T$  binning. Although our data favor GRV[5] or LAC1[4], none of them explain the high  $P_T$  excess ( $+1.5\sigma$  at  $P_T > 2.6$  GeV).

There are ambiguities in the above-mentioned theoretical predictions, which depend on  $m_c$  and  $\mu$ . We changed  $m_c$  from 1.3 to 1.8 GeV and  $\mu$  from  $m_c/2$  to  $2m_c$ . The lower  $m_c$  and  $\mu$  give a higher cross section which has a  $P_T$  dependence. The lowest  $P_T$  region may be explained by such ambiguities as mentioned above, and the threshold enhancement of  $c\bar{c}$  production. We thus concentrate on the higher  $P_T$  regions, i.e.,  $P_T > 2.6$  GeV. The case for  $m_c = 1.3$  GeV and  $\mu = m_c/2$  gives the highest one, i.e.,  $+0.54\text{pb}$  ( $+6\%$ ) higher than the nominal value. The experiment gives  $\sigma(2.6 < P_T < 6.6 \text{ GeV}) = 19.8 \pm 7.0\text{pb}$ , where the GRV parametrization predicts  $9.0 \pm 0.5$  pb. Then the difference is  $10.8 \pm 7.5\text{pb}$ .

In addition, if gluons inside the photon have  $P_T$ s of 0.4 GeV in average, the  $P_T$ s of  $c\bar{c}s$  are shifted. This may increase the resolved photon cross section by about a factor of two, because the spectrum of this process is proportional to an exponential function. Therefore, the  $2 \sim 3\text{pb}$  increase may be expected by this (no increase in the direct process). Then our results become consistent with the expectation within  $1 \sigma$  level.

Such event shapes as missing  $P_T$  and thrust distributions were checked. These shapes are consistent with the prediction of the lowest-order direct and resolved photon processes, except for the overall normalization factor.

In a part of the data set (integrated luminosity of  $90 \text{ pb}^{-1}$ ), there were forward calorimeters (FCL: made of BGO) which covered the polar angle region between 3.2 and 13.6 degrees [20]. We analyzed tagged events by the FCL with the same analysis. We observed the total  $D^{*\pm}$  yield to be  $3.5 \pm 3.6$ , where the lowest-order direct process predicts  $1.0 \pm 0.4$  events. We therefore need more statistics in order to observe tags from electrons and positrons as well as spectator jets.

In conclusion, we measured the inclusive  $D^{*\pm}$  production cross section in two-photon collision events at the TRISTAN  $e^+e^-$  collider. The mean  $\sqrt{s}$  was 57.16 GeV and the integrated luminosity was  $150 \text{ pb}^{-1}$ . We observed  $20 \pm 5$   $D^{*\pm}$  in our data sample. The production cross section in the high  $P_T$  region was  $\sigma_{D^{*\pm}}(2.6 < P_T < 6.6 \text{ GeV}) = 19.8 \pm 7.0\text{pb}$ . Comparisons with the theoretical prediction of the direct process and the resolved photon process were carried out.

We appreciate discussions with Prof. M. Kobayashi (KEK), Dr. M. Drees (Univ. of Wisconsin), M. Krämer (DESY), and J. Zunft (DESY). We thank the TRISTAN accelerator staff for the successful operation of TRISTAN. We also thank all engineers and technicians at KEK as well as members of the collaborating institutions: H. Inoue, N. Kimura, K. Shiino, M. Tanaka, K. Tsukada, N. Ujiie, and H. Yamaoka.

## References

- [1] See e.g. S. J. Brodsky, T. Kinoshita, and H. Terazawa, Phys. Rev. **D4** (1971) 1532.
- [2] D. W. Duke and J. F. Owens [DO], Phys. Rev. **D26** (1982) 1600.
- [3] M. Drees and K. Grassie [DG], Z. Phys. **C28** (1985) 451.
- [4] H. Abramowicz, K. Charchula, and A. Levy [LAC], Phys. Lett. **B269** (1991) 458.
- [5] M. Glück, E. Reya, and A. Vogt [GRV], Phys. Rev. **D46** (1992) 1973.
- [6] Ch. Berger et al., Z. Phys. **C33** (1987) 351; H. -J. Behrend et al., Z. Phys. **C51** (1991) 365; H. Aihara et al., Phys. Rev. **D41** (1990) 2667; R. Tanaka et al., Phys. Lett. **B277** (1992) 215.
- [7] M. Drees, M. Krämer, J. Zunft, and P. M. Zerwas, Phys. Lett. **B306** (1993) 371.
- [8] W. Bartel et al., Phys. Lett. **B184** (1987) 288.
- [9] W. Braunschweig et al., Z. Phys. **C47** (1990) 499.
- [10] M. Alston-Garnjost et al., Phys. Lett. **B252** (1990) 499.
- [11] R. Enomoto et. al., Nucl. Instrum. Methods, **A269** (1988) 507; A. Imanishi et. al., Nucl. Instrum. Methods, **A269** (1988) 513; T. Kamae et. al., Nucl. Instrum. Methods, **A252** (1986) 423; A. Yamamoto et. al., Jpn. J. Appl. Phys. Lett., **25** (1986) L440; S. Kawabata et. al., Nucl. Instrum. Methods, **A270** (1988) 11; J. Fujimoto et. al., Nucl. Instrum. Methods, **A256** (1987) 449; S. Noguchi et. al., Nucl. Instrum. Methods, **A271** (1988) 464.
- [12] H. Aihara et al., Phys. Rev. Lett., **53** (1984) 2465.
- [13] T. Sjöstrand, Comput. Phys. Commun., **39** (1986) 347; T. Sjöstrand and M. Bengtsson, Comput. Phys. Commun., **43** (1987) 367. The symmetric LUND fragmentation function with  $\sigma_q = 0.42$ ,  $a=0.9$ , and  $b=0.61$  without parton shower option was used. These parameters were fitted with single  $\gamma$  annihilation hadronic events, which was described in I. Adachi et al., Phys. Lett. **B227** (1989) 495. These parametrization also reproduce charm meson fragmentation function at lower energies.
- [14] H. Hayashii et al., Phys. Lett. **B314** (1993) 149.
- [15] “Review of Particle Properties”, Phys. Rev. **D45** (1992), Part II.
- [16] F. Butler et al., Phys. Rev. Lett. **69** (1992) 2041.
- [17] D. Decamp et al., Phys. Lett. **B266** (1991) 218.
- [18] D. Bortoletto et al., Phys. Rev. **D37** (1988) 1719; **D39** (1989) 1471.
- [19] J. Smith and W. van Neerven, Nucl. Phys. **B274** (1992) 36.
- [20] H. Hayashii et al., Nucl. Instrum. Method., **A316** (1992) 202.



This figure "fig1-1.png" is available in "png" format from:

<http://arxiv.org/ps/hep-ex/9411002v3>

This figure "fig1-2.png" is available in "png" format from:

<http://arxiv.org/ps/hep-ex/9411002v3>

This figure "fig1-3.png" is available in "png" format from:

<http://arxiv.org/ps/hep-ex/9411002v3>

This figure "fig1-4.png" is available in "png" format from:

<http://arxiv.org/ps/hep-ex/9411002v3>